Modulation of the Redox Potential of the [Fe(SCys)$_4$] Site in Rubredoxin by the Orientation of a Peptide Dipole†

Marly K. Eidsness,*,‡ Amy E. Burden,‡ Kimberly A. Richie,‡,§ Donald M. Kurtz, Jr.,‡ Robert A. Scott,‡ Eugene T. Smith,|| Toshiko Ichiye,⊥ Brian Beard,⊥ TongPil Min,⊥ and ChulHee Kang⊥

Department of Chemistry and Center for Metalloenzyme Studies, University of Georgia, Athens, Georgia 30602-2556, Department of Chemistry, Hamline University, St. Paul, Minnesota 55104-1284, and Department of Biochemistry and Biophysics, Washington State University, Pullman, Washington 99164-4660

Received July 20, 1999; Revised Manuscript Received September 8, 1999

ABSTRACT: Rubredoxins (Rds) may be separated into two classes based upon the correlation of their reduction potentials with the identity of residue 44; those with Ala44 have reduction potentials that are ∼50 mV higher than those with Val44. The smaller side chain volume occupied by Ala44 relative to that occupied by Val44 has been proposed to explain the increase in the reduction potential, based upon changes in the Gly43−Ala44 peptide bond orientation and the distance to the [Fe(SCys)$_4$] center in the *Pyrococcus furiosus* (Pf) Rd crystal structure compared to those of Gly43−Val44 in the *Clostridium pasteurianum* (Cp) Rd crystal structure. As an experimental test of this hypothesis, single-site Val44 ↔ Ala44 exchange mutants, [V44A]Cp and [A44V]Pf Rds, have been cloned and expressed. Reduction potentials of these residue 44 variants and pertinent features of the X-ray crystal structure of [V44A]Cp Rd are reported. Relative to those of wild-type Cp and Pf Rds, the V44A mutation in Cp Rd results in an 86 mV increase in midpoint reduction potential and the [A44V] mutation in Pf Rd results in a 95 mV decrease in midpoint reduction potential, respectively. In the crystal structure of [V44A]Cp Rd, the peptide bond between residues 43 and 44 is ∼0.3 Å closer to the Fe center and the hydrogen bond distance between the residue 44 peptide nitrogen and the Cys42 γ-sulfur decreases by 0.32 Å compared to the analogous distances in the wild-type Cp Rd crystal structure. The results described herein support the prediction that the identity of residue 44 alone determines whether a Rd reduction potential of about −50 or 0 mV is observed.

The simplest of the biological iron−sulfur centers is the [Fe(SCys)$_4$] site, which is prototypically found in a family of small (52−54-residue) proteins called rubredoxins (Rds).[1] These proteins occur widely in bacteria and archaea, and the available experimental evidence suggests that they function solely as electron-transfer agents (*1*, *2*). Approximately 14 known Rds share 50−60% sequence identity (*3*). All structurally characterized Rds have in common an essentially isostructural [Fe(SCys)$_4$] site of distorted tetrahedral FeS$_4$ coordination geometry and a nearly superimposable protein fold which are illustrated in Figure 1. A set of six (peptide)NH···γS(Cys) hydrogen bonds in the second coordination sphere (one of which is denoted in Figure 1) is also a conserved structural feature. The commonality of these structural features, the small size of Rds, and the large

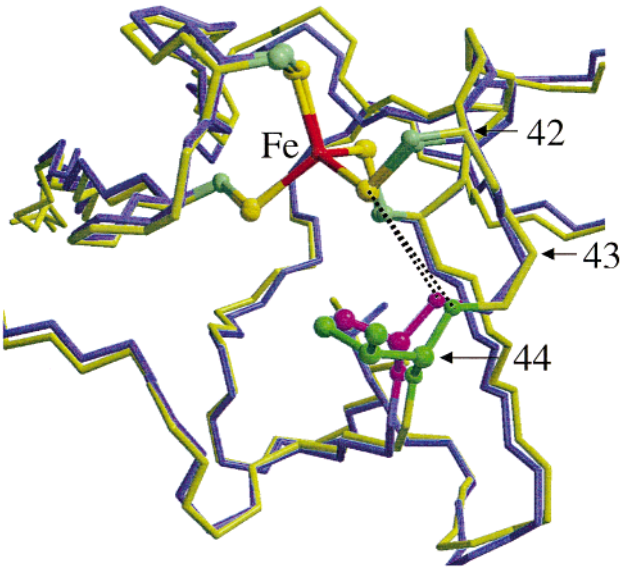

FIGURE 1: Superposition of Cp (yellow-green) and Pf (violet) Rd backbone structures comparing the orientations of the peptide bonds of Val44 in Cp Rd (green) and Ala44 in Pf Rd (magenta) near the Fe center (red) and cysteine-ligand sulfurs (yellow). Structures were generated using Molscript (*41*, *42*) and coordinates from PDB files 1IRN (*15*) and 1BRF (*14*). Numbers indicate the positions of α-carbons of residues 42−44 (using Cp Rd sequence numbering). Dashed lines represent (residue 44)NH···γS(Cys42) hydrogen bonds.

† Support for the work performed at the University of Georgia came from the National Institutes of Health (Grant GM50736) and the National Science Foundation Research Training Group Award to the Center for Metalloenzyme Studies (DIR 90-14281). E.T.S., T.I., and C.K. acknowledge support from the National Institutes of Health (Grants GM59030-01, GM45303, and GM53651, respectively).

* To whom correspondence should be addressed. E-mail: eidsness@uga.edu.

‡ University of Georgia.

§ Present address: Department of Physiology and Biophysics, University of Alabama at Birmingham, 1918 University Blvd., MCLM 893, Birmingham, AL 35294-0005.

|| Hamline University.

⊥ Washington State University.

[1] Abbreviations: Rd, rubredoxin; Cp, *Clostridium pasteurianum*; Pf, *Pyrococcus furiosus*; NHE, normal hydrogen electrode; *E*°′, midpoint reduction potential of the cyclic voltammogram; EPR, electron paramagnetic resonance.

10.1021/bi991661f CCC: $18.00
Published on Web 10/21/1999

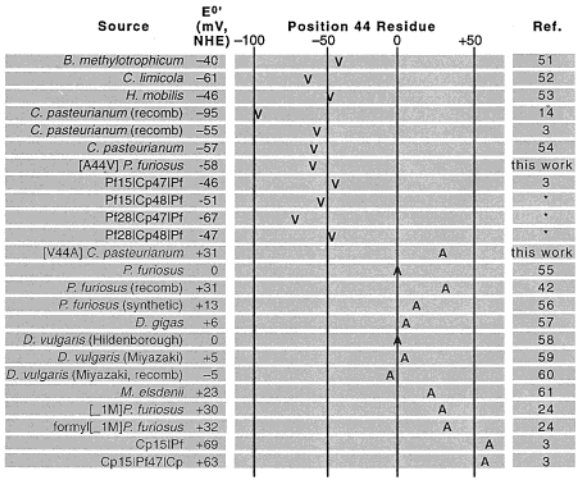

FIGURE 2: Reduction potentials of native and chimeric Rds grouped according to the identity of Ala or Val at position 44 (using Cp Rd numbering). All Rds with Val at position 44 have lower reduction potentials. *M. K. Eidsness, D. M. Kurtz, Jr., K. A. Richie, R. A. Scott, and E. T. Smith, unpublished experiments.

structural database (coordinates for Rds from six different species were deposited in the Protein Data Bank as of July 1999) have suggested that Rds could serve as a paradigm for analyzing the effects of the protein environment on redox potentials of non-heme metal centers.

The reduction potentials of the $[Fe(SCys)_4]^{1-/2-}$ couple among various Rds range between about −95 and 40 mV versus NHE (cf. Figure 2). This ~140 mV potential range for Rds could be extended to about 350 mV if the much higher reduction potential (~260 mV vs NHE) of the structurally very similar $[Fe(SCys)_4]$ center in rubrerythrin is included (*4*, *5*). These potentials may be compared to the value of about −800 mV versus NHE (measured in dimethylformamide) for the reduction potential of a synthetic $Fe(SR)_4^{1-/2-}$ complex (*6*, *7*). The ~800 mV difference in reduction potentials between the synthetic complex and the $[Fe(SCys)_4]$ sites in Rds has been attributed to the relatively close approach of peptide dipoles coupled with the low-dielectric environment within the protein (*6*, *8*, *9*). The smaller 140 mV range among the various Rds has been attributed to modulation by the positioning and orientation of peptide dipoles, whose positive ends are oriented toward the metal center (*10*−*12*).

Ichiye and co-workers (*10*) have pointed out that Rds may be separated into two classes on the basis of the correlation of their reduction potentials with the identity of residue 44 (using Cp Rd sequence numbering). Those with Ala44 have an $E^{\circ\prime}$ of ~0 mV, and those with Val44 have an $E^{\circ\prime}$ of about −50 mV versus NHE (Figure 2). In crystal structures of oxidized (i.e., Fe^{III}) *Desulfovibrio gigas* (Dg) and *Pyrococcus furiosus* (Pf) Rds, the Ala44 peptide nitrogen is ~0.4 Å closer to the Fe center than is the Val44 peptide nitrogen in oxidized Cp Rd [Figure 1; PDB file names 1RDG (*13*), 1BRF (*14*), and 1IRO (*15*), respectively]. This movement also shortens the (residue 44)N···γS(Cys42) hydrogen bond (represented by dashed lines in Figure 1) by ~0.3 Å. Variations in the NH···S distances could in principle modulate the $[Fe(SCys)_4]$ site redox potential by changing the covalency of the Fe−S bonds (*7*). However, no systematic correlation between Fe^{III}−S covalency and redox potential was found in Dg, Pf, and Cp Rds (*16*). An earlier crystallographic study showed negligible differences in the aforementioned distances between oxidized and reduced (i.e., Fe^{II}) Pf Rd (*17*). In fact, this study showed that minimal structural changes occur between the $[Fe(SCys)_4]^{2-}$ and $[Fe(SCys)_4]^{-}$ sites of Pf Rd, consistent with the idea that the Rd iron site has evolved to minimize its redox-induced reorganizational energy (*6*).

Ichiye and co-workers (*10*) proposed that the smaller volume occupied by the Ala44 relative to that of the Val44 side chain causes the observed decrease in the distance and the change in the orientation of the Gly43−Ala44 peptide bond with respect to the $[Fe(SCys)_4]$ site. These structural changes were proposed to increase the positive electrostatic contribution of the Gly43−Ala44 peptide dipole, and thus the reduction potential relative to those of Gly43−Val44 Rds. While the positioning of this single peptide dipole is the only significant structural difference near the iron site of Cp and Pf Rds, the amino acid sequences of the two classes of Rds differ at many positions other than residue 44. Among the Rds with the more negative potentials, a three-dimensional structure is available only for Cp Rd. To provide a more specific test of the hypothesis embodied in Figure 2, we prepared single-site Val44 ↔ Ala44 exchange mutants from each class, namely, [V44A]Cp Rd and [A44V]Pf Rd. In this paper, we report the characterization of these residue 44 variants, including measurements of their reduction potentials, and pertinent features of the X-ray crystal structure of [V44A]Cp Rd.

EXPERIMENTAL PROCEDURES

Cloning of [V44A]Cp and [A44V]Pf Rd Genes. [V44A]-Cp and [A44V]Pf Rd variant genes were made by the strand overlap extension (SOE) PCR method (*18*) using the wild-type Cp and Pf Rd genes in the pT7-7-derived plasmids, pNNQ (*19*) and pMKE-1 (*3*), respectively, as templates. The [V44A]Cp Rd gene was constructed using forward and reverse oligonucleotide primers with the sequence 5′-CTG TGC GGT **GCT** GGT AAA GAC-3′ (mutated codon shown in bold) and its reverse complement. The [A44V]Pf Rd gene was constructed in an analogous fashion, using oligonucleotide primers with the sequence 5′-ATC TGC GGT **GTT** CCG AAA TCC-3′ and its reverse complement. The mutated genes were constructed in two sections, one resulting from PCR amplification of the N-terminal portion using the T7 oligonucleotide primer (5′-TAATACGACTCACTATAGGG-3′) and either the [V44A]Cp Rd or the [A44V]Pf Rd reverse primer described above. The other section resulted from PCR amplification of the C-terminal portion of the gene using the oligonucleotide primer T7R (5′-TGGTAACTGTCA-GACCAAGTTTACTCA-3′), which duplicates the pT7-7 sequence downstream of the multiple cloning site, and either the [V44A]Cp Rd or the [A44V]Pf Rd forward primer. For the PCR experiments, we used 50 ng of template DNA, 50 pmol of each primer, *Pfu* DNA polymerase, dNTPs, and buffer in a 100 μL reaction volume, as recommended by Stratagene (La Jolla, CA). The PCR thermal cycle program for all SOE PCR amplifications was 60 s at 94 °C, followed by 45 cycles with the following sequence: 30 s at 94 °C, 30 s at 55 °C, and 30 s at 72 °C, and completed by 5 min at

72 °C. All PCR products were purified by QIAquick PCR Purification Kits (Qiagen, Inc., Chatsworth, CA) following the manufacturer's instructions. The purified PCR products were quantified by their absorbance at 260 nm in a Shimadzu UV-2101PC scanning spectrophotometer, using 1 cm path length quartz cuvettes. The final step in the SOE PCR consisted of fusion of the complementary N- and C-terminal PCR products. Equimolar amounts (ca. 50−100 ng) of N- and C-terminal ([V44A]Cp or [A44V]Pf Rd) PCR products were used as templates and combined with both T7 and T7R primers to amplify the [V44A]Cp or [A44V]Pf Rd genes. The PCR thermal cycle program was the same as the one given above. The final PCR products were purified with the QIAquick PCR purification kits.

The [V44A]Cp and [A44V]Pf Rd genes, as purified PCR products, were digested with restriction enzymes, *Nde*I and *Hin*dIII, and the digested Rd genes were extracted from a 2% Super Fine Resolution (SFR) agarose gel (Amresco, Solon, OH) and purified with a QIAEX II kit (Qiagen, Inc.). The digested, purified Rd genes were ligated into the *Nde*I and *Hin*dIII restriction sites of the overexpression vector pT7-7 (*20*) using 3 pmol of the gene and 0.06 pmol of pT7-7 (100 ng), following standard molecular biology procedures (*21*) to generate plasmids p[V44A]Cp and p[A44V]Pf. These plasmids were transformed into *Escherichia coli* strain 71/18 (*22*) for cloning and amplification. Nucleotide sequences of the Rd genes in Qiagen tip-100 purified p[V44A]Cp and p[A44V]Pf were verified by sequencing of both strands (using T7 and T7R primers) at the Molecular Genetics Instrumentation Facility at the University of Georgia.

Overexpression and Purification of [V44A]Cp and [A44V]-Pf Rds. The plasmids p[V44A]Cp and p[A44V]Pf were transformed into *E. coli* strain BL21(DE3) (Novagen, Inc., Madison, WI). Cultures were grown with shaking (300 rpm) at 37 °C in 6 L of Luria-Bertani medium supplemented with ampicillin (100 μg/mL) until the optical density at 600 nm reached 1.3−1.5, at which time 0.4 mM (final concentration) isopropyl β-D-thiogalactoside (IPTG) was added. The cultures were shaken for an additional 5 h at 37 °C and then harvested by centrifugation for 20 min at 6000*g*. The cell pellet was resuspended in 50 mL of 50 mM Tris-HCl buffer at pH 7.4. The cells were lysed by sonication (550 Sonic Dismembrator, Fisher Scientific), and the lysates were cleared by centrifugation at 27000*g* for 30 min.

Crude [V44A]Cp Rd or [A44V]Pf Rd was separated from *E. coli* proteins by passage over a QAE-Sephadex G-25 (Amersham Pharmacia Biotech) column, washed with 150 mM NaCl in 50 mM Tris-HCl at pH 7.4, and eluted with 500 mM NaCl in the same Tris buffer. The crude Rds were desalted and concentrated by ultrafiltration in an Amicon cell with a 3000 molecular mass cutoff membrane in 50 mM Tris-HCl at pH 7.4. In *E. coli*, both Fe (red-colored) and Zn (colorless) forms of Rds are overexpressed (*23*). The Zn- and FeRds were resolved by anion-exchange chromatography on a Mono-Q HR10/10 (Amersham Pharmacia Biotech) column connected to a Pharmacia FPLC system, as described in ref *3*. The chromatographic gradient for [V44A]Cp Rd was buffer A (25 mM Tris-HCl at pH 7.4) mixed with 20 to 40 vol % buffer B (buffer A with 1.0 M NaCl at pH 7.4) in a total elution volume of 75 mL; for [A44V]Pf Rd, the gradient was buffer A with 10 to 30 vol % buffer B in an elution volume of 75 mL. For [A44V]Pf FeRd, additional purification was required to separate three forms differing in their post-translational processing of the N-terminus (*24*, *25*), retaining the wild-type form (without the N-terminal Met) for this study. The additional purification steps consisted of a second passage over the same Mono-Q column using an elution gradient of buffer A with 20 to 30 vol % buffer B in an elution volume of 50 mL. This was followed by passage over a 10 mL hydroxyapatite column (CHT1, Bio-Rad, Richmond, CA) using a gradient of buffer C (5 mM sodium phosphate at pH 6.0) with 15 to 25 vol % buffer D (500 mM sodium phosphate at pH 6.0) in a total elution volume of 150 mL. After purification, [V44A]Cp and [A44V]Pf FeRds were desalted by ultrafiltration with a YM3 membrane with water, concentrated in YM3 Centricon tubes (Amicon) to ∼2 mM, and stored at −80 °C.

UV−Visible Absorption and EPR Spectroscopies. UV−visible absorption spectra were recorded on a Shimadzu UV-2101PC scanning spectrophotometer using 1 cm path length quartz cuvettes. The Rds were ca. 50 or 35 μM in 50 mM Tris-HCl at pH 8.5. Reduced Rds were generated using a deazaflavin catalyst followed by exposure to white light (*26*, *27*). To the oxidized Rds, a final deazaflavin concentration of 2 μM (from a 1 mM stock solution prepared in dimethylformamide) was added and the solution was deoxygenated on a N_2/vacuum manifold. The solution was then irradiated with white light from a slide projector at close range, and the UV−visible absorption spectrum was monitored until no further change occurred.

EPR spectra of oxidized [V44A]Cp and [A44V]Pf Rds were measured at the Electron Paramagnetic Resonance Spectroscopy Laboratory at the University of Georgia by I. Dhawan. X-band (∼9.6 GHz) EPR spectra of the 0.1 mM Rd samples (in 50 mM Tris-HCl at pH 8.5) were recorded on a Bruker ESP-300E EPR spectrometer with a dual-mode ER-4116 cavity equipped with an Oxford Instruments ESR-9 flow cryostat (4.2−300 K). Frequencies were measured with a frequency counter, and the field was calibrated with a Bruker ER 035M gaussmeter.

Mass Spectrometry of [V44A]Cp Rd and [A44V]Pf Rds. Molecular masses of [V44A]Cp Rd and [A44V]Pf Rd were determined by a combination of liquid chromatography and electrospray ionization mass spectrometry (LC−ESIMS) at the Chemical and Biological Sciences Mass Spectrometry Facility by D. Phillips. [V44A]Cp Rd and [A44V]Pf Rd samples were injected onto a Kromasil C-4 column (1 mm × 150 mm) with a 100 Å pore size and 5 mm particle size (Keystone Scientific Inc., Bellefonte, PA). Samples were analyzed using a PE-Sciex API 1 Plus mass spectrometer (Toronto, ON) coupled with an Applied Biosystems (API, Foster City, CA) 140B solvent delivery system and an API 759A absorbance detector. The mass spectrometer was scanned from 800 to 1500 amu using a 0.2 amu step and a 2.0 ms dwell time. The spray voltage was 4500 V, and the OR voltage was 60 V. Spectra were processed using PE Sciex software BioMultiView 1.2. Molecular masses of Rds were calculated by the program Peptidesort from Wisconsin Package Version 10.0 [Genetics Computer Group (GCG), Madison, WI].

Electrochemistry of [V44A]Cp Rd and [A44V]Pf Rds. A microelectrochemical cell composed of a pyrolytic graphite working electrode, a platinum counter electrode, and an Ag/AgCl reference electrode was used to obtain cyclic voltam-

mograms. The operation of the cell has been previously described (*28*). Prior to each experiment, the pyrolytic graphite electrode was polished in figure eights across a 60 μm aluminum oxide polishing wheel (Buehler, Lake Bluff, IL) moistened with water. The electrode was then rinsed with distilled water, and residual graphite was removed with lint free tissue. To remove O_2, the assembled electrochemical cell was flushed with N_2. A 10−20 μL anaerobic sample of approximately 100 μM protein in 0.1 M NaCl and 20 mM phosphate at pH 7 in a Hamilton gastight syringe was inserted through the cell septum and injected into the cell to form a drop between the working and reference electrode. Next, 2 μL of an electrode promoter, 0.1 M $MgCl_2$, was anaerobically added to this droplet. Cyclic voltammograms of Rds were recorded utilizing a CV-50W BAS voltammetric analyzer from 2 to 200 mV/s. Reduction potentials were determined from the midpoint between the anodic and cathodic peak currents. All reduction potentials are reported versus NHE.

X-ray Crystallography of [V44A]Cp Rd. Crystals of [V44A]Cp Rd were grown by the hanging drop vapor diffusion method from a solution containing 30 mg/mL protein and 0.05 M sodium acetate at pH 5.0. Drops with a volume of approximately 4 μL were equilibrated against a reservoir containing 0.1 M sodium acetate and 2.5 M ammonium sulfate. Crystals reaching a size of 0.2 mm × 0.2 mm × 0.3 mm were grown overnight. X-ray diffraction analysis revealed that the [V44A]Cp Rd molecule had crystallized in space group $P2_1$, where $a = 38.35$ Å, $b = 57.42$ Å, $c = 38.50$ Å, and $\beta = 112.74°$, and a volume of asymmetric unit large enough for approximately three molecules. The data set was collected on a Rigaku R-axis IIC imaging plate at 4 °C at a detector distance of 100 mm. The final R_{sym} value was 5%, generating 18 892 unique reflections above the 2σ level in the 15.0−1.6 Å resolution range.

The molecular replacement method, using X-PLOR (*29*), was used to determine the structure of [V44A]Cp Rd with the crystal structure of wild-type Cp Rd (PDB file name 1IRO) (*15*) as a starting model. Initially, a cross-rotational search with 15.0−2.4 Å data produced more than 90 unique orientations, whose rotation function (RF) value ranged from 0.27 to 0.23. Sixteen independent solution sets were left after a subsequent Patterson correlation stage by using 12.0−2.4 Å resolution range data. After translation searches with these various orientations using 3107 reflections from 15.0 to 3.0 Å resolution, three unique positions which contained no symmetry overlap were generated. These three positions of the Fe center were further confirmed by a MAD (*30*) data set collected at Brookhaven National Laboratory (Beamline X12C). The station was calibrated by locating the absorption edge of an $FeCl_2$ sample. The wavelengths were chosen by scanning through the absorption edge of a [V44A]Cp Rd crystal. All data were processed with DENZO (*31*). Initial rigid-body refinement was carried out using 5981 reflections from 15.0−2.4 Å resolution data and produced an R value of 40.3%. After several cycles of positional refinement, temperature factor refinement, and simulated annealing omit map calculations, the R factor for the final model containing 380 non-hydrogen atoms was 17.6% ($R_{free} = 20.5\%$) for 6914 reflections above the 2σ level between 8.0 and 2.2 Å resolution. The rms deviation is 0.01 Å for bonds and 2.417° for angles. One hundred fifty-three water molecules are included in the structure. The coordinates were deposited in the Brookhaven Protein Data Bank (file name 1C06).

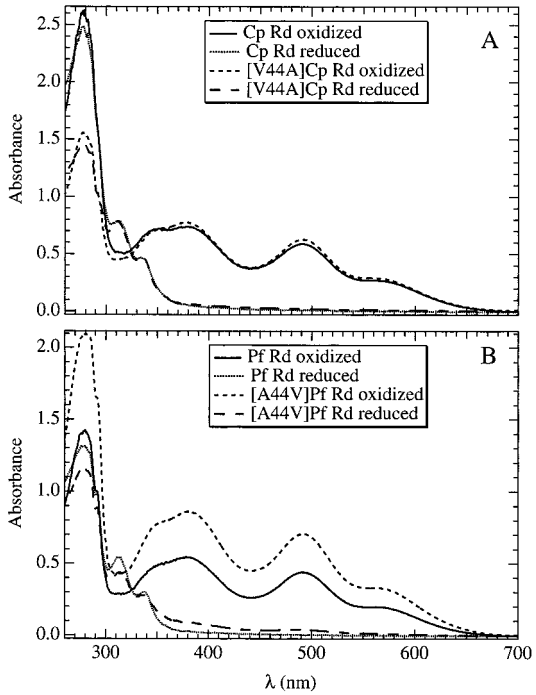

FIGURE 3: UV−visible absorption spectra of oxidized and reduced Rds. Wild-type Cp, [A44V]Pf, and [V44A]Cp Rd concentrations were ca. 50 μM, and the Pf Rd concentration was ca. 35 μM in 50 mM Tris-HCl at pH 8.5. Reduced Rds were generated with a deazaflavin catalyst (see Experimental Procedures).

RESULTS

Mass Spectrometry. The molecular masses of [V44A]Cp and [A44V]Pf Rds were determined by electrospray ionization mass spectrometry to be 6019.0 and 5923.0 Da, respectively. Calculated molecular masses of apo-[V44A]-Cp and apo-[A44V]Pf Rd are 6018.6 and 5923.5 Da, respectively, including an N-terminal methionine residue for the Cp Rd, but not for the Pf Rd. Under the ionization conditions that were used, the apo forms are expected to be the predominant ions (*3*). The close agreement between calculated and experimentally determined molecular masses verifies the residue 44 mutations.

UV−Visible Absorption and EPR Spectra. The UV−visible absorption spectra of oxidized and reduced [V44A]-Cp and [A44V]Pf Rd and the EPR spectra of the oxidized Rds were measured to determine whether the structures of the pseudotetrahedral $Fe^{III,II}S_4$ sites of wild-type Cp and Pf Rds were significantly perturbed by the residue 44 mutations. The absorption spectra of the oxidized Rds (cf. Figure 3) show the characteristic S → Fe charge-transfer transitions in the visible region with maxima at ca. 380, 490, and 580 nm (*6*). The reduced Rds have no absorbance in the visible region but are characterized by two absorption features at ca. 315 and 335 nm (*19*). The close resemblance of the UV−visible absorption spectra of the wild-type and mutated Rds indicate that the residue 44 mutations have not significantly perturbed either the oxidized or the reduced FeS_4 centers. This conclusion is supported by the EPR spectra of oxidized [V44A]Cp and [A44V]Pf Rds (cf. Figure 4). The spectra exhibit characteristic features at $g = 4.3$ and 9.6 which have

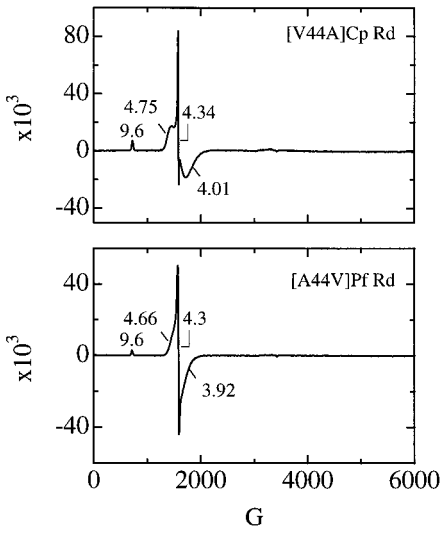

FIGURE 4: X-Band EPR spectra of oxidized [V44A]Cp (top) and [A44V]Pf Rds (bottom) measured with microwave powers of 2.0 and 1.0 mW, respectively. Rd samples (0.1 mM in 50 mM Tris-HCl at pH 8.5) were assessed at 4 K.

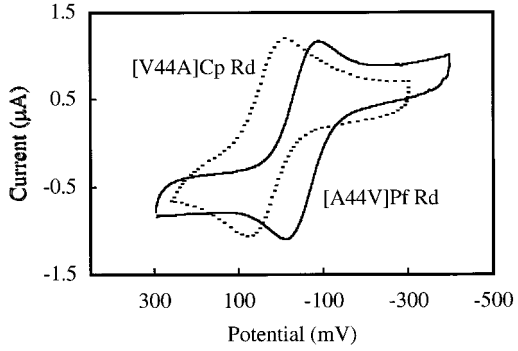

FIGURE 5: Cyclic voltammograms of [A44V]Pf (solid lines) and [V44A]Cp (dashed lines) Rds in 0.1 M NaCl and 50 mM phosphate buffer at pH 7.6. The Rd concentration was ca. 0.1 mM, and the scan rate was 4 mV/s.

been assigned to transitions of a nearly rhombic $S = {}^5/_2$ site (*32*). These features are essentially identical in the EPR spectra of the wild-type and mutated Rds.

Electrochemistry. Cyclic voltammograms of [V44A]Cp and [A44V]Pf Rds and the corresponding wild-type Pf Rd (*33*) were recorded (cf. Figure 5). The midpoint reduction potential (vs NHE) of the [V44A]Cp Rd was 31 mV, compared with −55 mV for wild-type Cp Rd previously measured under the same conditions (*19*). Thus, the V44A mutation in Cp Rd results in an 86 mV increase in midpoint reduction potential. The [A44V]Pf Rd midpoint reduction potential was determined to be −58 mV, compared with 37 mV for wild-type Pf Rd, giving a 95 mV decrease in midpoint reduction potential for the A44V mutation in Pf Rd. These results support the hypothesis based on the data depicted in Figure 2 that reduction potentials of Rds are significantly more positive when residue 44 is Val rather than Ala, and further indicate that residue 44 alone is responsible for this reduction potential shift.

X-ray Crystallography of [V44A]Cp Rd. The crystals of [V44A]Cp Rd were assumed to be in the Fe^{III} form on the basis of their red color. The basic coordination geometry of the [Fe(SCys)$_4$] site, including the second sphere NH···γS-(Cys) hydrogen bonding pattern of the ligand residues, is

Table 1: Comparison of Distances for Residues 43 and 44 in Pf Rd, Cp Rd, and [V44A]Cp Rd

	44N−Fe (Å)	43O−Fe (Å)	44N−S42 (Å)
Pf Rd (1CAA)	4.81	6.99	3.49
Cp Rd (1IRO)	5.24	7.30	3.84
[V44A]Cp	4.90 ± 0.015[a]	7.07 ± 0.055[a]	3.52 ± 0.032[a]

[a] Values are the means of the three molecules in the crystallographic asymmetric unit and their rms values.

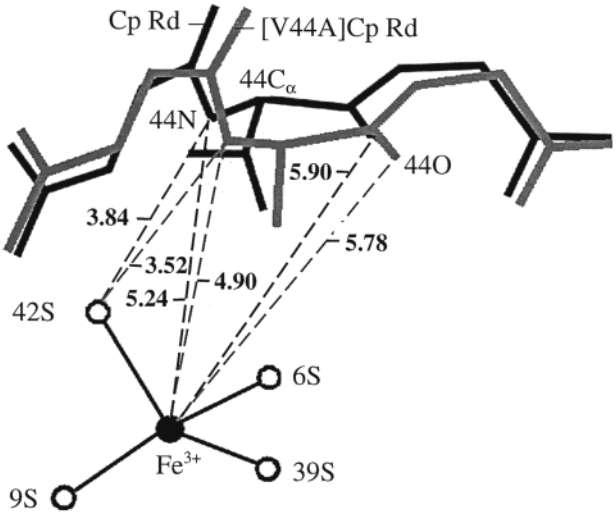

FIGURE 6: Comparison of distances (in angstroms) from the iron center to the peptide backbone of residue 44 and from the Cys42 sulfur to the residue 44 amide nitrogen in Cp Rd (black) and [V44A]-Cp Rd (gray).

essentially unaffected by the V44A mutation. However, significant structural changes at residue 44 were found in [V44A]Cp Rd (see Table 1 and Figure 6). In the crystal structure, three independent [V44A]Cp Rd molecules are observed. The average rms difference between the three independent [V44A]Cp Rd molecules in the asymmetic unit and wild-type Cp Rd of the backbone atoms (residues 1−50 only) is 0.22 Å. The average distance between the Ala44 peptide nitrogen atoms and the Fe centers in the three independent molecules is 4.90 ± 0.015 Å. These distances are all significantly shorter than the corresponding (Val44)-NH···Fe distances previously determined in the wild-type Cp Rd crystal structure [5.24 Å; PDB file name 1IRO (*15*)], but similar to that in the Pf Rd crystal structures [4.81 and 4.84 Å; PDB file names 1CAA (*17*) and 1BRF (*14*), respectively]. Similar bond length decreases exist between the Gly43 carbonyl oxygen atoms and the Fe center (see Table 1). Thus, the peptide bond between residues 43 and 44 is ca. 0.3 Å closer to the Fe center when residue 44 is Ala rather than Val.

The V44A mutation in Cp Rd also shortens the hydrogen bond distance between the residue 44 peptide nitrogen and the Cys42 γ-sulfur by an average of 0.32 ± 0.03 Å compared to that of wild-type Cp Rd (3.84 Å). This hydrogen bond shortening is not accompanied by a significant change in the (Cys42)γS−Fe bond distance [average of 2.21 Å in [V44A]Cp Rd vs 2.23 Å in wild-type Cp Rd (*15*)] or by significant changes in the other Fe−γS(Cys) or NH···S structural parameters. Full details of the structural refinement of the [V44A]Cp Rd crystal structure will be published elsewhere (C. Kang, manuscript in preparation).

DISCUSSION

The ability of the protein environment to tune redox potentials of metal sites could allow for evolutionary adaptation in specific electron transport systems. Differential stabilization by the protein of one member of a redox couple has been variously ascribed to (1) solvent exposure (or lack thereof) (*34*), (2) the control of ligand residue arrangement (the "rack" or entatic state) (*35*), (3) specific hydrogen bonding networks (*36*), (4) the proximity and orientation of protein-based dipoles (*37*), (5) the proximity of charged residues (*10*, *38*), or (6) the metal−ligand covalency, which modulates the effective nuclear charge of the metal ion (*6*, *16*). Since the basic pseudotetrahedral $[Fe(SCys)_4]$ geometry and (peptide)NH···γS(Cys) hydrogen bonding pattern is retained in all structurally characterized Rds, redox tuning via ligand residue rearrangement would appear to be negligible. A significant change in Fe−S covalency (mechanism 6) in our mutated Rds also seems unlikely given the lack of perturbation of the $Fe^{II,III}(SCys)_4$ spectroscopic parameters. The remaining mechanisms are all derived from straightforward mono- or dipolar electrostatic effects.

Coulombic electrostatics predicts that adding positively charged residues near the metal site should favor electron addition, thereby raising the metal site reduction potential. However, earlier studies by us (*19*) and others (*39*) found that varying charges on surface residues do not modulate the iron site redox potential in Rd in a manner predicted by these simple Coulombic electrostatic considerations. The other three mechanisms for redox potential tuning (mechanisms 1, 3, and 4 in the above list) can all be understood in terms of stabilization of a charged metal site (an electric monopole) by oriented dipoles, either on the protein or in solvent.

The results described herein support and extend the prediction by Ichiye and co-workers (*10*) that the identity of residue 44 alone determines whether a Rd reduction potential of about −50 or 0 mV is observed. In fact, our measurements show that substitution of Ala for Val at residue 44 raises the redox potential of Rd by ∼90 mV. The crystal structure of [V44A]Cp Rd also confirms the predicted movement of the peptide bond connecting residues 43 and 44. Substitution of the isopropyl side chain of Val with the methyl side chain of Ala results in both movement of this peptide dipole 0.3 Å closer to the iron and a shortening of the (residue 44)NH···γS(Cys42) hydrogen bond by ∼0.3 Å. This movement of the positive end of the peptide dipole closer to the $[Fe(SCys)_4]$ site within the relatively low-dielectric environment of the protein should preferentially stabilize the more negatively charged $[FeII(SCys)_4]^{2-}$ site. Our electrochemical measurements confirm the preferential stabilization of the reduced iron site in [V44A]Cp Rd, and of the oxidized site in [A44V]Pf Rd.

Wedd and co-workers (*40*) found that the [G43V]Cp Rd variant exhibits a reduction potential that is ca. 50 mV more negative than that of Cp Rd, and the ^{1}H chemical shift of the V44 NH proton in the ^{113}Cd-substituted variant undergoes a large upfield shift of −0.36 ppm compared to small shifts of other amide proton resonances in the vicinity of the chelating loop formed by residues 38−44. In the absence of a [G43V]Cp Rd crystal structure, one can speculate that the perturbation of the V44 amide proton environment and the lower reduction potential could be due to displacement of the V44 amide farther from the Fe center, as this work would predict. Alternatively, envelopment of the Val43 side chain in a more hydrophobic environment would be expected to favor a lower reduction potential.

For our [V44A] and [A44V] Rds, contributions in addition to movement of the peptide dipole would seem to be relatively minor. Increased exposure of the $[Fe(SCys)_4]$ site to solvent water accompanying the Val → Ala substitution seems unlikely, given how well the Ala methyl group in [V44A]Cp Rd occupies the space previously occupied by the Val side chain. In the crystal structure of Cp Rd [PDB file name 1IRO (*15*)], the Val44 propyl side chain is in close contact with the propyl side chain of Val8 in a 90° orientation, leading to the four C_γ atoms of the two residues being all within 4.2 Å of each other. In [V44A]Cp Rd, the C_β atom of Ala44 has moved to within 4.2 Å of the C_γ atoms of Val8. This movement suggests different amounts of hydrophobic or van der Waals forces in the local structures of the two molecules, which could conceivably provide a different magnitude in water shielding capacity. The agreement between theory and experiment embodied in this work exemplifies progress in deconvoluting the factors that control protein redox potential tuning.

ACKNOWLEDGMENT

C.K. thanks C. Ogata for help with synchrotron data collection.

NOTE ADDED IN PROOF

After completion of this work, we became aware of a similar set of experiments on Cp Rd carried out by Wedd and co-workers (*43*). Their results are consistent with ours.

REFERENCES

1. Eggink, G., Engel, H., Vriend, G., Terpstra, P., and Witholt, B. (1990) *J. Mol. Biol. 212*, 135−142.
2. Gomes, C. M., Silva, G., Oliveira, S., LeGall, J., Liu, M. Y., Xavier, A. V., Rodrigues-Pousada, C., and Teixeira, M. (1997) *J. Biol. Chem. 272*, 22502−22508.
3. Eidsness, M. K., Richie, K. A., Burden, A. E., Kurtz, D. M., Jr., and Scott, R. A. (1997) *Biochemistry 36*, 10406−10413.
4. Gupta, N., Bonomi, F., Kurtz, D. M., Jr., Ravi, N., Wang, D. L., and Huynh, B. H. (1995) *Biochemistry 34*, 3310−3318.
5. de Maré, F., Kurtz, D. M., Jr., and Nordlund, P. (1996) *Nat. Struct. Biol. 3*, 539−546.
6. Holm, R. H., Kennepohl, P., and Solomon, E. I. (1996) *Chem. Rev. 96*, 2239−2314.
7. Bair, R. A., and Goddard, W. A., III (1978) *J. Am. Chem. Soc. 100*, 5669−5676.
8. Yang, Y., Beck, B. W., Shenoy, V. S., and Ichiye, T. (1993) *J. Am. Chem. Soc. 115*, 7439−7444.
9. Yelle, R. B., Park, N. S., and Ichiye, T. (1995) *Proteins 22*, 154−167.
10. Swartz, P. D., Beck, B. W., and Ichiye, T. (1996) *Biophys. J. 71*, 2958−2969.
11. Stephens, P. J., Jollie, D. R., and Warshel, A. (1996) *Chem. Rev. 96*, 2491−2513.
12. Swartz, P. D., and Ichiye, T. (1997) *Biophys. J. 73*, 2733−2741.
13. Frey, M., Sieker, L., Payan, F., Haser, R., Bruschi, M., Pepe, G., and LeGall, J. (1987) *J. Mol. Biol. 197*, 525−541.
14. Bau, R., Rees, D. C., Kurtz, D. M., Jr., Scott, R. A., Huang, H., Adams, M. W. W., and Eidsness, M. K. (1998) *JBIC, J. Biol. Inorg. Chem. 3*, 484−493.

15. Dauter, Z., Wilson, K. S., Sieker, L. C., Moulis, J. M., and Meyer, J. (1996) *Proc. Natl. Acad. Sci. U.S.A. 93*, 8836−8840.
16. Rose, K., Shadle, S. E., Eidsness, M. K., Kurtz, D. M., Jr., Scott, R. A., Hedman, B., Hodgson, K. O., and Solomon, E. I. (1998) *J. Am. Chem. Soc. 120*, 10743−10747.
17. Day, M. W., Hsu, B. T., Joshua-Tor, L., Park, J.-B., Zhou, Z. H., Adams, M. W. W., and Rees, D. C. (1992) *Protein Sci. 1*, 1494−1507.
18. Horton, R. M., Hunt, H. D., Ho, S. N., Pullen, J. K., and Pease, L. R. (1989) *Gene 77*, 61−68.
19. Zeng, Q. D., Smith, E. T., Kurtz, D. M., Jr., and Scott, R. A. (1996) *Inorg. Chim. Acta 242*, 245−251.
20. Tabor, S. (1990) in *Current Protocols in Molecular Biology* (Ausubel, F. A., Brent, R., Kingston, R. E., Moore, D. D., Seidman, J. G., Smith, J. A., and Struhl, K., Eds.) pp 16.2.1−16.2.11, Greene Publishing and Wiley-Interscience, New York.
21. Ausubel, F. M., Brent, R., Kingston, R. E., Moore, D. D., Seidman, J. G., Smith, J. A., and Struhl, K. (1992) *Current Protocols in Molecular Biology*, Greene Publishing and Wiley-Interscience, New York.
22. Messing, J., Gronenborn, B., Müller-Hill, B., and Hofschneider, P. H. (1977) *Proc. Natl. Acad. Sci. U.S.A. 74*, 3642−3646.
23. Richie, K. A., Teng, Q., Elkin, C. J., and Kurtz, D. M., Jr. (1996) *Protein Sci. 5*, 883−894.
24. Ben-Bassat, A., Bauer, K., Chang, S.-Y., Myambo, K., Boosman, A., and Chang, S. (1987) *J. Bacteriol. 169*, 751−757.
25. Dalbøge, H., Bayne, S., and Pedersen, J. (1990) *FEBS Lett. 266*, 1−3.
26. Massey, V., Stankovich, M., and Hemmerich, P. (1978) *Biochemistry 17*, 1−8.
27. Massey, V., and Hemmerich, P. (1978) *Biochemistry 17*, 9−17.
28. Smith, E. T., Bennett, D. W., and Feinberg, B. A. (1991) *Anal. Chim. Acta 251*, 27−33.
29. Brunger, A. T. (1992) *X-PLOR A system for crystallography and NMR*, version 3.1, Yale University Press, New Haven, CT.
30. Hendrickson, W. A. (1990) *Science 254*, 51−58.
31. Otwinowski, Z., and Minor, W. (1997) *Methods Enzymol. 276*, 307−326.
32. Peisach, J. (1971) *J. Biol. Chem. 246*, 5877−5881.
33. Gillès de Pélichy, L. D., and Smith, E. T. (1999) *Biochemistry 38*, 7874−7880.
34. Capozzi, F., Ciurli, S., and Luchinat, C. (1998) *Struct. Bonding 90*, 127−160.
35. Wittung-Stafshede, P., Hill, M. G., Gomez, E., Bilio, A. J. D., Karlsson, B. G., Leckner, J., Winkler, J. R., Gray, H. B., and Malmström, B. G. (1998) *JBIC, J. Biol. Inorg. Chem. 3*, 367−370.
36. Adman, E., Watenpaugh, K. D., and Jensen, L. H. (1975) *Proc. Natl. Acad. Sci. U.S.A. 72*, 4854−4858.
37. Sham, Y. Y., Muegge, I., and Warshel, A. (1998) *Biophys. J. 74*, 1744−1753.
38. Warshel, A., and Papazyan, A. (1998) *Curr. Opin. Struct. Biol. 8*, 211−217.
39. Kümmerle, R., Zhuang-Jackson, H., Gaillard, J., and Moulis, J. M. (1997) *Biochemistry 36*, 15983−15991.
40. Ayhan, M., Xiao, Z., Lavery, M. J., Hamer, A. M., Nugent, K. W., Scrofani, S. D. B., Guss, M., and Wedd, A. G. (1996) *Inorg. Chem. 35*, 5902−5911.
41. Merritt, E. A., and Murphy, M. E. P. (1994) *Acta Crystallogr. 50D*, 869−873.
42. Kraulis, P. (1991) *J. Appl. Crystallogr. 24*, 946−950.
43. Xiao, Z., Maher, M., Lucarelli, M., Gardner, A., Guss, M., and Wedd, A. G. (1999) *J. Inorg. Biochem. 74*, 335−335.

BI991661F